

Applications of wavelets and neural networks for classification of power system dynamics events

Samir AVDAKOVIC^{1,*}, Amir NUHANOVIC², Mirza KUSLJUGIC²,
Elvisa BECIROVIC¹

¹Department for Development, EPC Elektroprivreda B&H D.D. Sarajevo, Sarajevo, Bosnia and Herzegovina

²Department of Power Systems Analysis, Faculty of Electrical Engineering, University of Tuzla,
Tuzla, Bosnia and Herzegovina

Received: 27.06.2012 • Accepted: 08.11.2012 • Published Online: 17.01.2014 • Printed: 14.02.2014

Abstract: This paper investigates the possibility of classifying power system dynamics events using discrete wavelet transform (DWT) and a neural network (NN) by analyzing one variable at a single network bus. Following a disturbance in the power system, it will propagate through the system in the form of low-frequency electromechanical oscillations (LFEOs) in a frequency range of up to 5 Hz. DWT allows the identification of components of the LFEO, their frequencies, and magnitudes. After determining the energy components' share of the analyzed signal using DWT and Parseval's theorem, the input data for the classification process using a NN are obtained. A total of 5 classes of disturbances, 3 different wavelet functions, and 2 different variables are tested. Simulation results show that the proposed approach can classify different power disturbance types efficiently, regardless of the choice of variable or wavelet function.

Key words: Power system dynamics, low-frequency electromechanical oscillations, wavelet transform, neural network, disturbance

1. Introduction

A power system is a complex, dynamic system, composed of a large number of interrelated elements, where some elements are merely the system's components while others affect the whole system [1–5]. Several large-scale blackouts of power systems have occurred worldwide over the past 10 years. One of the largest in European history was the collapse of the electricity power system in Italy, on 28 September 2003, resulting in the loss of electricity for 57 million people. An analysis of these collapses indicates that the most common causes are the chain propagation of the initial disturbance with high intensity and some failures in operation and power system planning [6]. The modern approach to power system monitoring, operation, and control involves the fast and accurate identification and localization of the disturbance. Accurate and fast automatic identification of the disturbance type and location can help the system operator with the proper initiation of corrective actions that would eliminate or reduce the impact of disturbances on the system. Generally, the objectives of disturbance identification are to detect the onset in time of disturbance, classify the type of disturbance, estimate the disturbance intensity and damping, and estimate the end time of the disturbance and the type and location of the initial event [7]. The classification of signals that carry specific information about disturbances involve the use of different artificial intelligence techniques, such as fuzzy logic (FL), artificial neural networks (ANNs), and adaptive FL, or techniques based on probabilistic models [8]. On the other hand, wavelet transform (WT) is a

*Correspondence: s.avdakovic@elektroprivreda.ba

relatively new mathematical area that is applied in various areas of science, and several papers present successful WT applications in combination with other techniques that relate to the classification of signal processes [9–15]. In electrical engineering, there are vast numbers of papers in the field of power system measurement, partial discharges, and power system transients, protection, or quality. There are fewer papers related to the WT analysis of electromechanical dynamic phenomena in power systems and they are mainly related to disturbance identification and the analysis and identification of low-frequency electromechanical oscillations (LFEOs) in power systems, as well as the identification and estimation of an active power unbalance in the power system [16–28].

A new approach for the classification of power system dynamic events based on WT and a neural network (NN) is proposed in this paper. Discrete wavelet transform (DWT) with multiresolution analysis (MRA) is applied to decompose signals of electromechanical transient oscillation in a frequency range of up to 5 Hz. DWT with MRA allows the identifications of power system LFEOs and the determination of their frequencies and magnitudes. Following the identification of LFEOs in the signal that are coming out of the DWT filters, Parseval’s theorem is used to determine the energy share of the signal DWT decomposition levels, whose values represent the input to the NN used for classification. Five classes of power system disturbances, which can represent higher intensity disturbances, are analyzed as follows: loss of generation units, line outage, 3-phase short circuit (TPSC), TPSC with a line outage, and TPSC with a line outage and unsuccessful reclosing. The classification performances of different wavelet functions [Daubechies4 (Db4), symlet4 (sym4), and biorthogonal3.3 (bior3.3)] and different variables (voltage angle and voltage magnitude) are tested.

The paper is organized in the following way: Section 2 is a presentation of the theoretical background and proposed methodology. Section 3 presents computer simulation and classification results of the proposed approach. Finally, conclusions are presented in Section 4.

2. Theoretical background and proposed methodology

The basic idea of the proposed methodology is based on the identification component of the LFEOs of the power system and determining their effects on the observed variables using DWT. The LFEOs of a power system are in the range of up to 5 Hz [5]. The block diagram for the power system events classification proposed in this paper is presented in Figure 1.

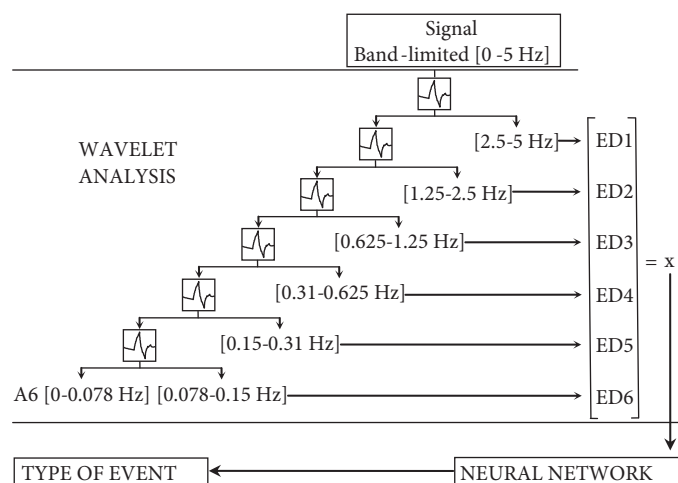


Figure 1. Block diagram for power system events classification.

The first step is the selection of analyzed variables and the definition of the measured signal sampling frequency. Considering the time and frequency range of electromechanical transients of power systems, as referred to in [2,4], it is common for them to be observed on a time scale of a few seconds and in a frequency range of up to 5 Hz. Selecting a signal sampling time of 0.1 s or sampling frequency of 10 Hz, it will include all frequencies in the range of up to 5 Hz and thus will eliminate electromagnetic transients from the signal that will be significantly reduced by the number of signal samples.

The second step is the DWT analysis of the selected signal. The dynamic response of a power system following a disturbance is characterized by significant fluctuations of the angles between the generators. The oscillations of the angles between the generators cause oscillations of the angles and magnitudes of the voltage in the power system buses as well as fluctuations in the power transmission lines. Different disturbances cause different power system responses. Accordingly, different classes of power system disturbances will have different effects on the LFEOs on the observed variables. The effects of the LFEOs on the selected variables are determined by the magnitude of the signals in the frequency ranges defined by the DWT and MRA implementation and are shown as the energy value of the signal at the DWT decomposition's different levels. Generally, the frequency band $[f_m/2 : f_m]$ of each DWT detail scale is directly related to the sampling rate of the original signal, which is given by $f_m = f_s/2^{l+1}$, where f_s is the sampling frequency and l is the decomposition level. DWT is a recursive process of filtering input data series by low-pass and high-pass filters. Outputs are scaling coefficients (approximations) and wavelet coefficients (details). Approximations are low-frequency components on large scales, and the details are high-frequency components of the function on small scales. DWT uses 2 digital filters: a low-pass filter, $h(n), n \in Z$, defined by scaling function $\varphi(x)$, and a high-pass filter, $g(n), n \in Z$, defined by wavelet function $\psi(x)$. Filters $h(n)$ and $g(n)$ are connected by a scaling function and wavelet function, respectively [9,16,29–32]:

$$\varphi(x) = \sum_n h(n) \sqrt{2} \varphi(2x - n), \tag{1}$$

$$\psi(x) = \sum_n g(n) \sqrt{2} \varphi(2x - n), \tag{2}$$

where $\sum_n h(n)^2 = 1$, $\sum_n g(n)^2 = 1$ and $\sum_n h(n) = \sqrt{2}$, $\sum_n g(n) = 0$

At the start of the filtering process is the separation of the approximations and details of the discrete signals, thus obtaining 2 signals. Digital signal $f(n)$, with a frequency band as in Figure 1 (0–5 Hz), is passed through the low-pass filter $h(n)$ and the high-pass filter $g(n)$. Each filter permits only half of the frequency spectrum of the original signal. Next, the filtered signals are subsampled so that every second sample is removed. Wavelet coefficients of j th level can be expressed through the approximation coefficients of the $j - 1$ level, as follows:

$$cA_j(k) = \sum_n h(2k - n) cA_{j-1}(n) , \tag{3}$$

$$cD_j(k) = \sum_n g(2k - n) cA_{j-1}(n) . \tag{4}$$

The coefficients $cA_j(k)$ are called approximations of the j th decomposition level and represent the input signal for the following frequency range. Analogously, $cD_j(k)$ are coefficients of details on the j th level. Decomposition continues in such a way that the coefficients of approximation $cA_j(k)$ are filtered through $g(n)$ and $h(n)$, i.e.

are separated on the approximations of the coefficients and the details in the following decomposition level and in accordance with the frequency range, as shown in Figure 1. As the algorithm continues, or, more precisely, as one goes toward lower frequencies, the number of samples decreases, which worsens the time resolution since a lower number of samples represents the entire signal for a given frequency range. However, the frequency resolution is improved as the frequency range where the signal is observed is narrower. Finally, the signal is decomposed on 6 decomposition level, as presented in Figure 1. Details D1–D6 represent 6 signals in a wide enough frequency range from 0.078 Hz up to 5 Hz, where all of the dominant components of the LFEO will be identified. The low-frequency component of signal A6 represents the trend of the observed signal after the disturbance and its energy value is usually much greater than the sum of the energies of all of the signals in detail. The low-frequency A6 component of the signal will not be used as input to the NN.

Furthermore, in order to reduce the number of input data in the NN, using Parseval's theorem, the energy values of these signals are calculated according to:

$$ED_i = \sum_{j=1}^N |D_{ij}|^2, \quad i = 1, 2, 3, 4, 5, 6. \quad (5)$$

Here, $i = 1, 2, 3, 4, 5, 6$ is the wavelet decomposition level from levels 1 to 6 and N is the number of detail coefficients at each decomposition level. ED_i is the energy of the detail at decomposition level i .

Finally, after DWT, which is the input for the NN, we get the 6-dimensional feature vector $x = [ED_1, ED_2, ED_3, ED_4, ED_5, ED_6]^T$ for the future analysis and classification process.

The third step is the classification of the disturbances by the NN. There are several types of NNs that can be used in the classification process. In this study, a feedforward NN (FFNN) is used. Generally, for ANNs, it is common that the accumulated knowledge during training can be utilized properly for some subsequent events. The FFNN consists of an input layer, output layer, and hidden layers. The connections have multiplying weights associated with them. Specifically, determining the number of neurons and hidden layers is a common problem in the NN method implementation. The process of determining the parameters of the NN is called the training process, during which the sets of input and output data are associated by proper adjustment of the weights in the network and the sum of the squared error function is minimized. The training process involves a specified learning rule. More details on the types and architectures of NNs can be found in the literature [33–36].

3. Computer simulation results

The simulation and analysis presented in this paper were performed using the New England (NE) 39-bus test system presented in Figure 2. The NE 39-bus test system consists of 10 generators connected at buses 30 to 39, where bus 31 is a slack bus. All of the generators are equipped with identical automatic voltage regulators (AVRs) and turbine governors (TGs). The loads are modeled as voltage-dependent loads. The load and line data of the test system come from [37], and the AVR and TG parameters come from [38]. The performance of the proposed approach was evaluated by the Power System Analysis Toolbox [39] and Wavelet Toolbox [40].

For the signal spectral analyses, a sampling time of 0.1 s or sampling frequency of 10 Hz of the original signal is chosen. Based on the Nyquist theorem, the highest frequency that the signal could contain might be $f_s/2$, i.e. 5 Hz. The frequency range of the decomposed signal in 6 decomposition levels is presented in Figure 1. Within 6 decomposition levels, as defined in the signal details (D1–D6), the dominant modes of the LFEO will be determined, including their magnitudes. The following 5 classes of power system disturbances are analyzed:

C1, loss of generation; C2, line outage; C3, TPSC; C4, TPSC with line outage; and C5, TPSC with line outage and unsuccessful reclosing.

In every simulated power system disturbance case, the voltage angle and voltage magnitude signals at bus 16 are observed in a 10-s simulation time frame. Bus 16 is chosen randomly as one of the central buses. The start of the disturbance in each simulated case is at 0.1 s and all of the voltage angle signals are presented in relation to bus 39.

Just for illustration, when speaking about the identification of the LFEO and the comparison of the different methodologies, we analyze 1 simulated TPSC disturbance case on bus 7, starting at 5.1 s and ending at 5.2 s. The total simulation time is 30 s, as taken just for illustration. After the disturbance simulation, oscillations are observed throughout the system. Figure 3 shows the voltage angle oscillations on bus 16 after the TPSC on bus 7.

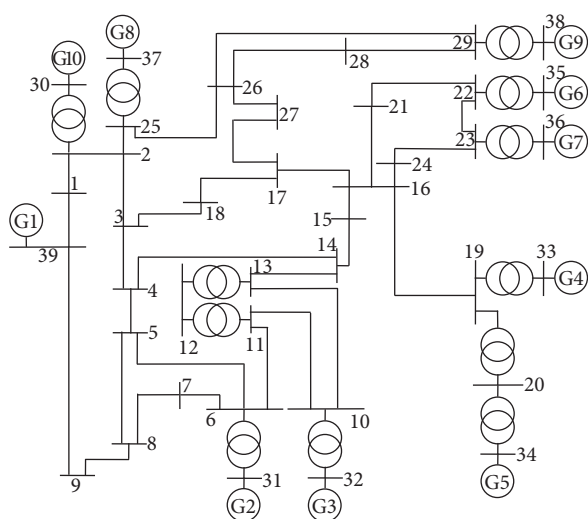


Figure 2. NE 39-bus test system.

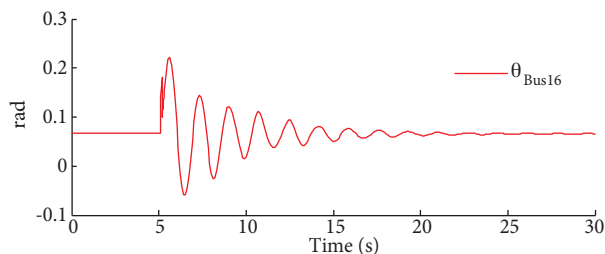


Figure 3. Voltage angle oscillations on bus 16 after the TPSC on bus 7.

It is clear from the signal observed in Figure 3 during the TPSC interval that a smaller transient is present, but after the disturbance clearance, the system continues to oscillate. It is obvious that the oscillations are damped, but some components might not be damped, even if it cannot be seen from the observed signal [17,18]. In a case where we observe the voltage magnitude, the transient or ‘sag’, the actual voltage magnitude decrease would be substantially higher due to the nature of the QV process during the short circuit.

Generally, the process of identification and monitoring of LFEOs is a very important task for power system operators. This can be performed using several different approaches, providing a different insight into the dynamic behavior of the power system. An efficient numerical method to evaluate LFEOs is based on eigenvalue analysis. However, the limitations of this approach are related to the interpretation of the results and demanding calculations for large networks. A more convenient approach is based on the direct analysis of the available signals, and methodologies that are often encountered in the literature are based on the Fourier transformation, Prony approach, WT, etc. A detailed comparison of the different approaches of identification and analysis of LFEOs can be found in [16–18,23,25,28]. The results of different approaches in the identification of LFEOs for the analyzed signal from Figure 3 are shown in Figures 4–7. The results of the fast Fourier transform (FFT) analysis, as shown in Figure 4, indicate that for the analyzed signal, the dominant frequency

component is 0.6 Hz. The main disadvantage of this approach is the loss of information about the beginning of a disturbance, i.e. the loss of information about which frequency is present in a certain time frame.

The results of the analysis of the signal from Figure 3 using the Prony approach are shown in Figure 5 and also indicate the dominant frequency of 0.6 Hz. This approach would not only get the characteristic frequencies, but also their damping. By modal form signal representation, one can find the corresponding amplitudes and also evaluate the energy contribution of the signal components. However, this method loses the information about the beginning of a power system disturbance.

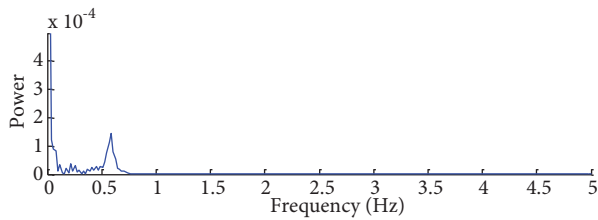


Figure 4. FFT results of the signal from Figure 3.

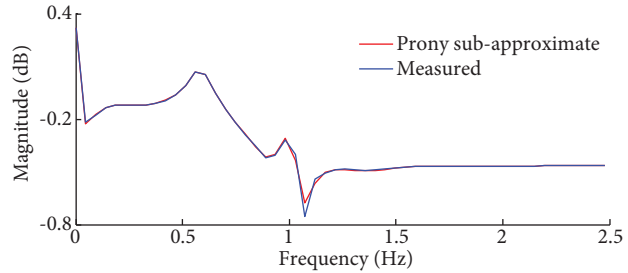


Figure 5. Prony approach results of the signal from Figure 3.

WT provides an excellent time-frequency analysis and the ability of local signal analysis. It also enables the usage of a longer time interval for the ‘capture’ of information about low-frequency components, and shorter time intervals for information about high-frequency components. The wavelet power spectrum and global wavelet spectrum of the signal results from Figure 3 are presented in Figure 6. Moreover, the dominant frequency component is 0.6 Hz, but in addition to information about the low-frequency components, this approach enables us to visualize the beginning of an underlying disturbance that presents important information for power system operators. The results of this approach are achieved using software tools available at <http://paos.colorado.edu/research/wavelets/>.

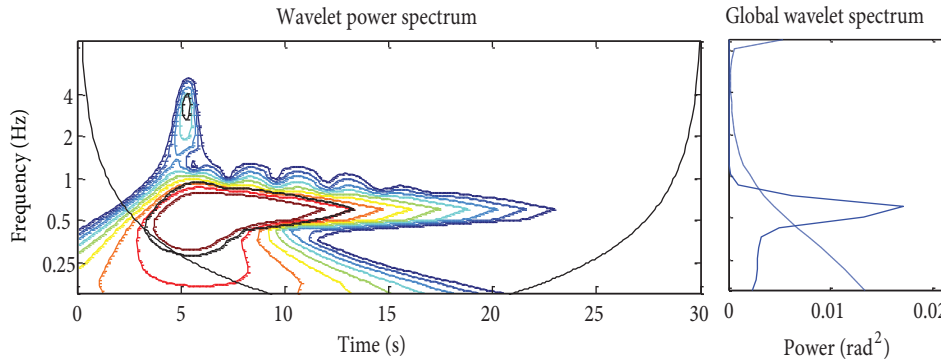


Figure 6. Wavelet power spectrum and global wavelet spectrum results of the signal from Figure 3.

The signal DWT from Figure 3 with the Db4 wavelet function is shown in Figure 7. The D1–D6 signals or outputs of the previously defined filters and A6 approximation signal that represents the signal low-frequency component with a frequency range of 0–0.078 Hz are shown. The first level of the signal decomposition (D1) is commonly used for identification of the disturbance start, as presented in Figure 7. The magnitude of this signal is quite small, and soon after the disturbance, it becomes a zero value. The signal second level decomposition (D2) corresponds to the local oscillations with small magnitude and damped characters. In the

other decomposition levels D3–D6, the intraarea or interarea oscillations can be identified with larger or smaller magnitudes. It is obvious that all oscillations are damped in this case, but the signal magnitudes in the third and the fourth decomposition levels are the largest. In addition, the A6 component obviously has the largest magnitude and represents the trend of the signal after a disturbance. In physics, the low-frequency component of a (power system) frequency signal represents a great estimation of the rate of change of the weighted average frequency (frequency of the center of inertia) [16], and, in this case, where you observe the angle difference of components A6 and with $A6/2\pi$, it should be close to the absolute change of the weighted average frequency.

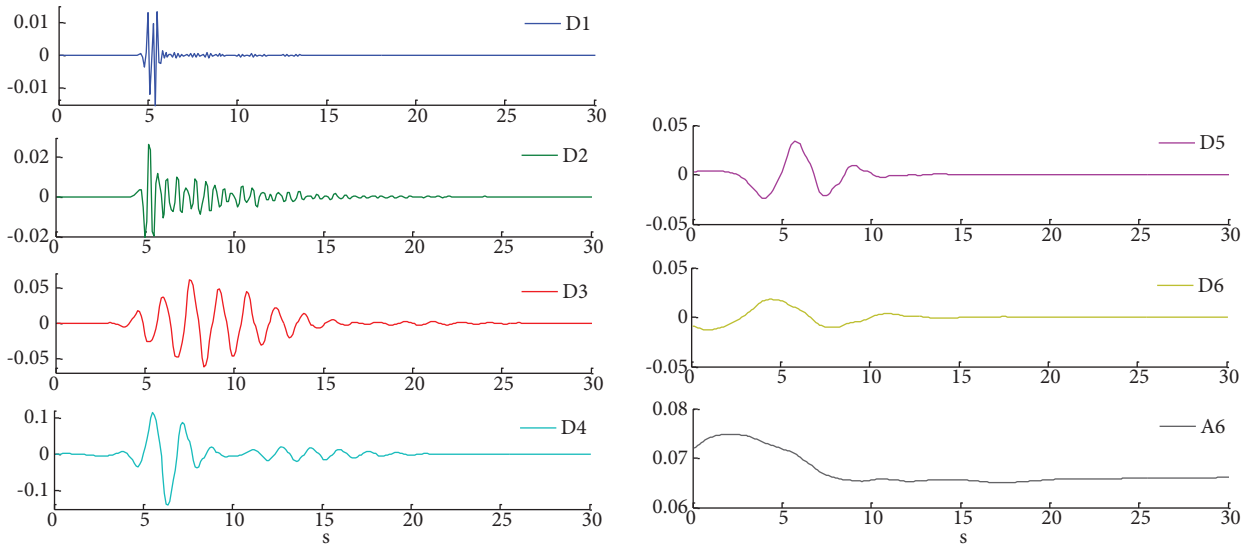


Figure 7. DWT results of the signal from Figure 3.

Herein, it is evident that the dominant frequency component is 0.6 Hz. In relation to the continuous wavelet transform, DWT provides a more simple application in practical engineering problems. Moreover, DWT provides the determination of energy shares of individual components in the overall signal. Thus, Figure 8 shows the energy percentage distribution in details D1–D6 and using the Db4 wavelet function (for the time period between 5 and 15 s for the signal from Figure 3) that is the image of the LFEO effect, following a disturbance in the observed variables. These values represent vector x , which is to be the input in the NN and the classification process.

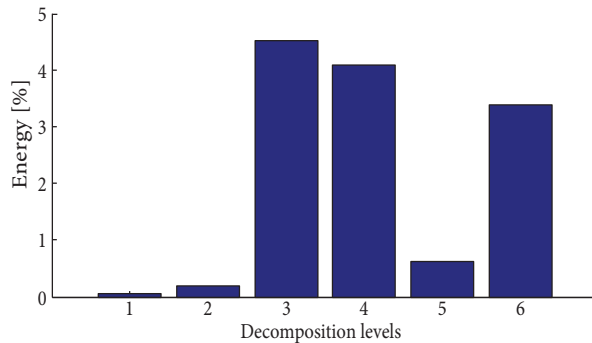


Figure 8. Percentage value of the signal component energy from Figure 3 for the D1–D6 decomposition levels.

The results of the simulation, calculation, and classification for a total of 140 analyzed disturbances are given below. During the analysis, 5 classes of disturbances, C1–C5, are identified, i.e. C1, 7 cases; C2, 34 cases; C3, 39 cases; C4, 34 cases; and C5, 26 cases.

Energy distribution diagrams of voltage angle signals at bus 16 for different disturbance cases in the power system are shown in Figures 9–13. Energy distribution diagrams of the voltage magnitude signals at bus 16 for different disturbance cases in the power system are shown in Figures 14–18.

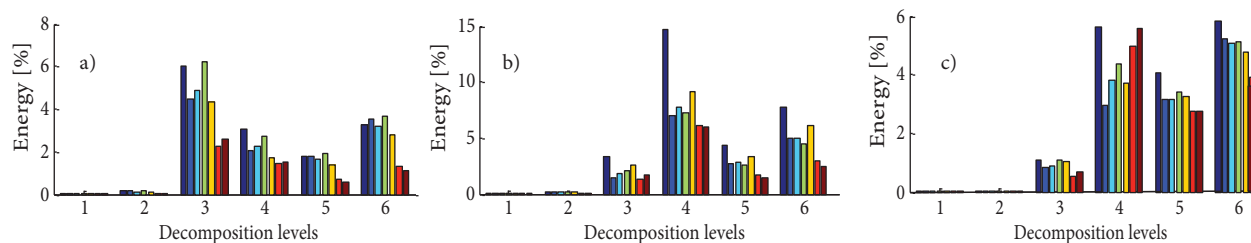


Figure 9. Energy distribution diagram of the voltage angle signal at bus 16 in case C1 with support: a) Db4, b) sym4, and c) bior3.3.

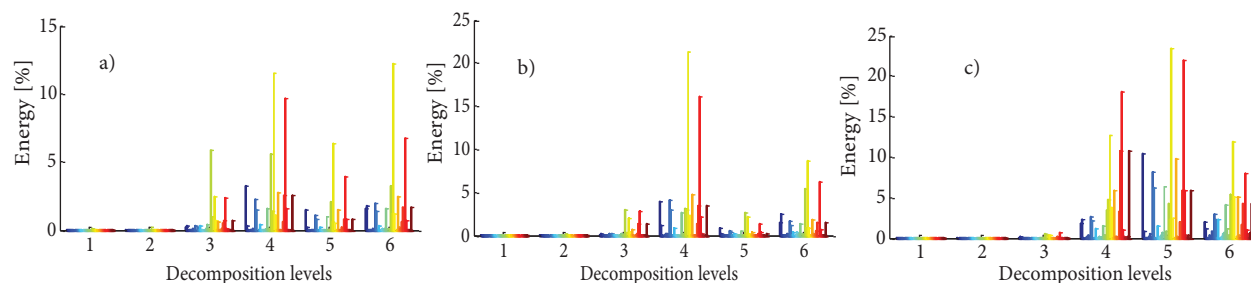


Figure 10. Energy distribution diagram of the voltage angle signal at bus 16 in case C2 with support: a) Db4, b) sym4, and c) bior3.3.

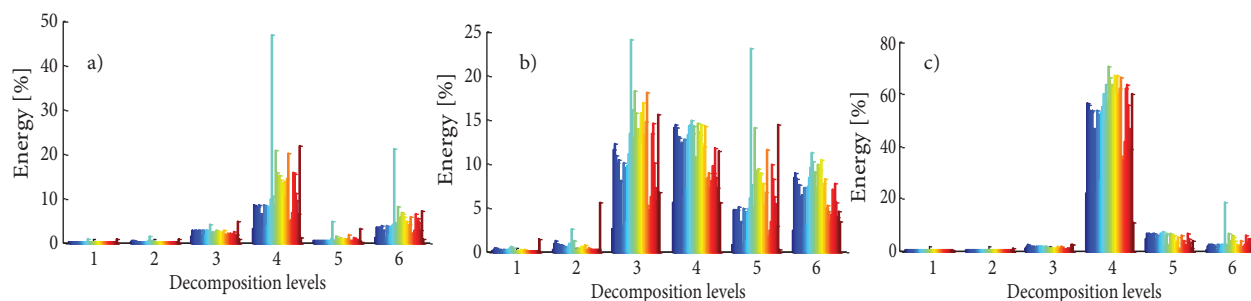


Figure 11. Energy distribution diagram of the voltage angle signal at bus 16 in case C3 with support: a) Db4, b) sym4, and c) bior3.3.

The analyses are performed for the Db4, sym4, and bior3.3 wavelet functions. It is generally difficult to find recommendations in the literature as to which function is the best for such analyses, but the change of the wavelet functions will certainly have an impact on the final energy distribution of the analyzed signal. This is evident from Figures 9–18.

By analyzing the energy distribution in detail, which refers to the calculations related to the voltage angle signals (Figures 9–13), it is evident that the signal components in the first 2 decomposition levels are rather small, and are far lower in relation to the other levels. Here, it is obvious that the components of the lower frequencies are dominant, and their percentage share in the total signal varies from one disturbance to another.

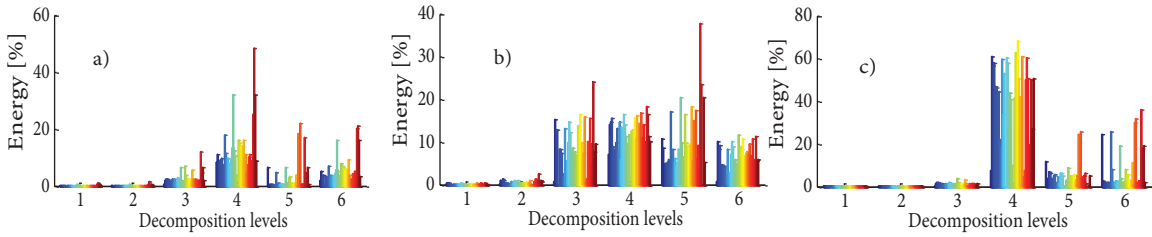


Figure 12. Energy distribution diagram of the voltage angle signal at bus 16 in case C4 with support: a) Db4, b) sym4, and c) bior3.3.

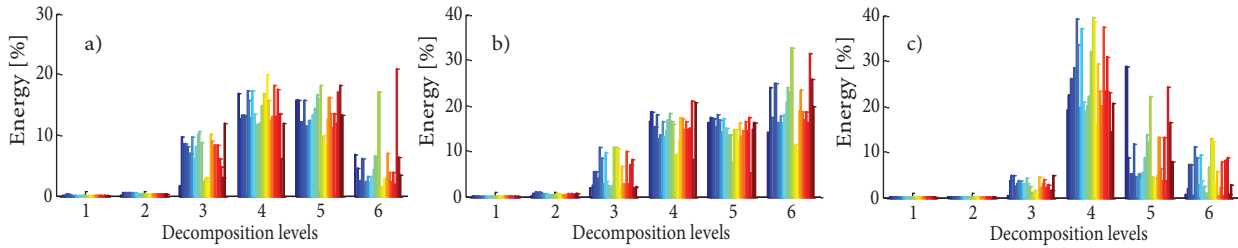


Figure 13. Energy distribution diagram of the voltage angle signal at bus 16 in case C5 with support: a) Db4, b) sym4, and c) bior3.3.

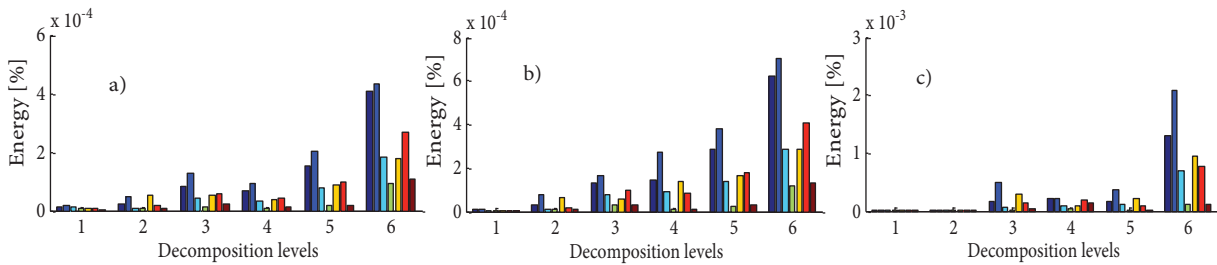


Figure 14. Energy distribution diagram of the voltage magnitude signal at bus 16 in case C1 with support: a) Db4, b) sym4, and c) bior3.3.

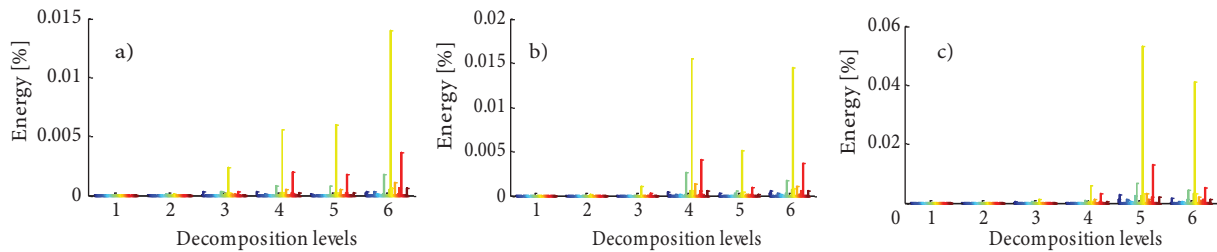


Figure 15. Energy distribution diagram of the voltage magnitude signal at bus 16 in case C2 with support: a) Db4, b) sym4, and c) bior3.3.

The results of the energy distribution of the voltage signal magnitude are slightly different, and their share in the total signal is reduced due to a lower influence of the LFEO on the voltage magnitude. It is obvious that the minimum values are for disturbances C1 and C2 (Figures 14 and 15), whereas these values are significantly higher for disturbances C3, C4, and C5 (Figures 16, 17, and 18) as the result of a ‘higher intensity’ disturbance in relation to the first 2, primarily disturbances that have significant impact on the reactive power flow. Moreover, due to the short circuit, the voltage magnitude will identify a larger ‘sag’, which will affect a

higher energy value in the first decomposition level. If one looks in more detail at the actual values of the energy, one can notice that they are grouped in layers with certain values of energies, i.e. for one type of disturbance, these are grouped around certain values that are extremely small. Furthermore, the shares of the energy signal components for C2 are higher than those for C1, but also much smaller for the other 3 disturbances. This is a good basis for the training and classification process in the NN.

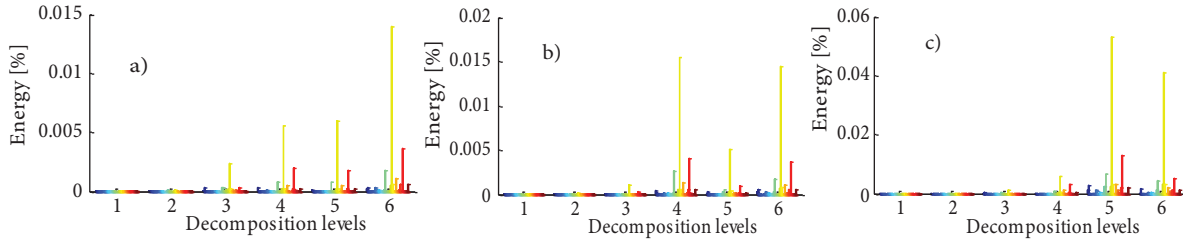


Figure 16. Energy distribution diagram of the voltage magnitude signal at bus 16 in case C3 with support: a) Db4, b) sym4, and c) bior3.3.

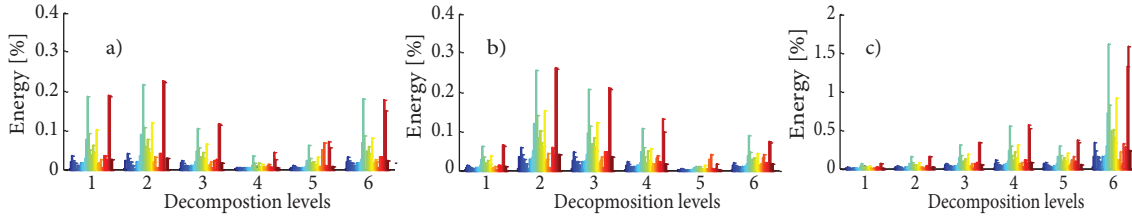


Figure 17. Energy distribution diagram of the voltage magnitude signal at bus 16 in case C4 with support: a) Db4, b) sym4, and c) bior3.3.

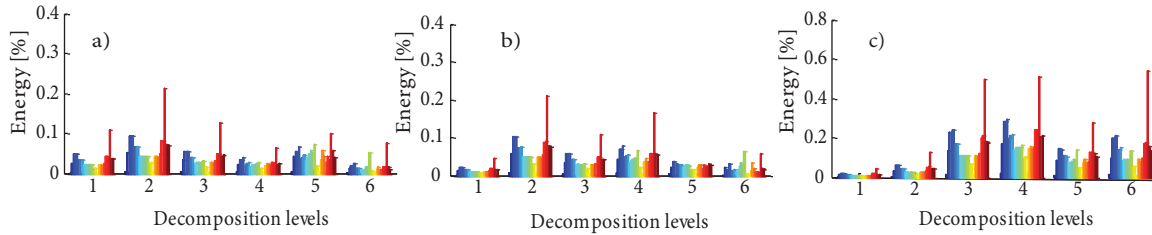


Figure 18. Energy distribution diagram of the voltage magnitude signal at bus 16 in case C5 with support: a) Db4, b) sym4, and c) bior3.3.

Finally, the NN architectures for all of the cases and the results of the classification with the FFNN are presented in the Table. They are selected to obtain the best performance after several different simulation cases, such as the number of hidden layers and hidden layer sizes. Data for each simulation case are selected randomly, where 90 data sets are used to train the NN model and 50 data sets are used for the testing process.

The classified accuracy rate of the distorted voltage angle signals and selected wavelet functions is 78%–82%. A high percentage of correct classification rates is obtained for 3 classes of disturbances signals, for cases C1, C2, and C5. The reason for the lower classification accuracy of the other cases (C3 and C4) might be that the energy distribution of those analyzed signals is quite similar (Figures 11 and 12).

The classified accuracy rate of the distorted voltage magnitude signals and selected wavelet functions ranges between 74% and 86%. The results vary among the cases, but it can be noted that the results of the

classification for 3 simulated cases, C2, C3, and C5, are slightly better for the disturbances compared to the disturbances of C1 and C4.

Table. NN architecture and classification results of the proposed algorithm.

Variable: voltage angle (θ_{16})																				
Wavelet function						Db4	Wavelet function						sym4	Wavelet function						bior3.3
The number of layers						4	The number of layers						4	The number of layers						4
The number of neurons on the layers						[6 6 4 1] ¹	The number of neurons on the layers						[6 7 4 1]	The number of neurons on the layers						[6 7 5 1]
Class	C1	C2	C3	C4	C5	Accuracy (%)	Class	C1	C2	C3	C4	C5	Accuracy (%)	Class	C1	C2	C3	C4	C5	Accuracy (%)
C1	2	0	0	0	0	100	C1	3	1	0	0	0	75	C1	4	0	0	0	0	100
C2	0	7	0	1	0	87.5	C2	0	10	0	0	0	100	C2	0	12	0	0	0	100
C3	0	1	10	6	0	58.8	C3	0	3	6	1	0	60	C3	0	0	12	1	0	92.3
C4	0	0	2	9	0	81.8	C4	0	0	4	10	0	71.43	C4	0	0	7	3	2	25
C5	0	0	0	0	12	100	C5	0	1	1	0	10	83.3	C5	0	0	0	0	9	100
Overall success rate						80.0	Overall success rate						78.0	Overall success rate						82.0
Variable: voltage magnitude (V_{16})																				
Wavelet function						Db4	Wavelet function						sym4	Wavelet function						bior3.3
The number of layers						4	The number of layers						4	The number of layers						4
The number of neurons on the layers						[6 7 6 1]	The number of neurons on the layers						[6 8 5 1]	The number of neurons on the layers						[6 8 6 1]
Class	C1	C2	C3	C4	C5	Accuracy (%)	Class	C1	C2	C3	C4	C5	Accuracy (%)	Class	C1	C2	C3	C4	C5	Accuracy (%)
C1	1	1	0	0	0	50	C1	0	2	0	0	0	0	C1	3	0	0	0	0	100
C2	0	12	1	0	0	92.3	C2	0	6	1	0	0	85.7	C2	0	9	3	0	0	75
C3	0	0	12	0	0	100	C3	0	0	20	0	0	100	C3	0	0	11	3	0	78.5
C4	0	0	10	5	1	31.2	C4	0	0	3	11	1	73.3	C4	0	0	8	5	0	38.5
C5	0	0	0	0	7	100	C5	0	0	0	0	6	100	C5	0	0	0	0	8	100
Overall success rate						74.0	Overall success rate						86.0	Overall success rate						72.0

¹[input: 6, the first inner layer: 6, the second inner layer: 6, output: 1]

It is possible to notice that the results of the analyzed voltage angle variable vary slightly for the 3 selected wavelet functions. With regard to analyzing the voltage magnitude variable and for the 3 selected wavelet functions, the results for some of the simulated disturbances vary. Thus, in the classification results for case C1, of 3 analyzed cases, the results vary from 0% to 100%.

Generally, for the 140 analyzed disturbances simulated on the test system, we can say that the results of the classification are sufficiently good. However, a logical question arises: What about the other power system disturbances that occur at almost any moment, such as the loss of load or loss of distribution lines? Five analyzed disturbances in this paper, however, represent disturbances with high intensity in power systems, which could have significant consequences for the system and, ultimately, along with the development of adverse events following a disturbance and protection operation, could lead to the formation of islands or the total collapse of the power system. Simply by setting thresholds for the energy value components of DWT signals, low-intensity disturbances can be eliminated [40].

Better results in terms of the classification results should be looked at by more careful selection of each element of the training set, using the appropriate tools for their filtering, in order to avoid over-fitting and an eventual increase of the variance results during the network testing. A technique of factor analysis (principal component analysis) could be applied in this or a similar analysis in order to possibly reduce the number of input variables, with no significant reduction in the total variability in the data. Although the FFNN is commonly used in the literature because of its simplicity setting, easier automation of the network selection, and its application, it is possible to find a successful application of a large number of other types of classifiers. In the case of the FFNN, the optimal choice of hidden layers and the number of neurons per layer might have an important role in the process of classification. In the case of over-fitting, it may happen that the training is

done very successfully, but for a variety of architectures of the FFNN, one gets different variances during the network testing, thus making the classification inconvenient.

Radial basis function, cascade NN, and Kohonen NN are some of the NNs that can be applied in the classification process. Since there are no general rules for the election of the classifier, for each specific problem, and even for that analyzed in this article, the specific analysis with different types of classifiers would advise the possible choice of one classifier that gives the best results.

4. Conclusions

In this paper, using DWT and a NN, the possibility of the classification of high-intensity disturbances in a power system was analyzed by observing one variable at a single network bus. The proposed approach is based on the identification of the dominant low-frequency components of the analyzed signal and determination of their participation with energy in the signal by DWT. From the performed simulations, analyses, and classifications, the following conclusions can be drawn.

Defining the sampling frequency of the signal and the number of DWT decomposition levels, one creates a 'space' where the observations for the disturbances are made like 6 output signals from the DWT, in which the magnitudes and frequencies of the LFEO after the disturbance will be identified.

The LFEO will arise in the system after the disturbance. The magnitude of these modes will, among other things, depend on the type of disturbance. Different wavelet functions of the DWT of the analyzed signals give different output signals from the filters, which affect the energy distribution for different frequency bands. However, it is obvious that the selection of the wavelet function does not affect the classification results. Furthermore, an important aspect of the proposed approach is the selection of the variables. Although the impact of the LFEO is reflected more in the variable of the voltage angle than in the voltage magnitude, the results of the classification for the 2 analyzed variables are approximately the same. Somewhat larger variations, however, in the classification results for a particular disturbance are evident for the analyzed variable of the voltage magnitude. Generally, regardless of the choice of wavelet functions or variables, the proposed approach gives relatively good results of classification. In the practical implementation of similar classifiers, one can often encounter problems related to the capacity and costs of necessary equipment. The classifier proposed in this paper is relatively simple, with a very low number of input data, and allows for the classification of disturbances that are relatively distant from the measurement location of the analyzed variable.

The subject of future research in the area of classification of high-intensity disturbances in power systems and improvement of the accuracy of classification results will be the application of different methods of input signal processing, infinite impulse response-based filters in wavelet decomposition, and a more complex NN architecture. Moreover, the testing of other artificial intelligence techniques in the classification process is reserved for future research.

References

- [1] P.M. Anderson, A.A. Fouad, *Power System Control and Stability*, 2nd ed., New York, Wiley-IEEE Press, 2002.
- [2] P. Kundur, *Power System Stability and Control*, New York, McGraw-Hill, 1994.
- [3] M. Ilić, J. Zaborszky, *Dynamics and Control of Large Electric Power Systems*, New York, Wiley, 2000.
- [4] J. Machowski, J.W. Bialek, J.R. Bumby, *Power System Dynamics and Stability*, New York, Wiley, 1997.
- [5] B. Pal, B. Chaudhuri, *Robust Control in Power Systems*. New York, Springer, 2005.

- [6] V. Madani, D. Novosel, A. Apostolov, S. Corsi, “Innovative solutions for preventing wide area cascading propagation”, *Bulk Power System Dynamics and Control*, pp. 729–750, 2004.
- [7] P. Kundur, J. Paserba, V. Ajjarapu, G. Andersson, A. Bose, C. Canizares, N. Hatziargyriou, D. Hill, A. Stankovic, C. Taylor, T. Van Cutsem, V. Vittal, “Definition and classification of power system stability IEEE/CIGRE joint task force on stability terms and definitions”, *IEEE Transactions on Power Systems*, Vol. 19, pp. 1387–1399, 2004.
- [8] P. Settipalli, *Automated Classification of Power Quality Disturbances Using Signal Processing Technique and Neural Network*, PhD, University of Kentucky, Lexington, KY, USA, 2007.
- [9] H. He, J.A. Starzyk, “A self-organizing learning array system for power quality classification based on wavelet transform”, *IEEE Transactions on Power Delivery*, Vol. 21, pp. 286–295, 2006.
- [10] Z.L. Gaing, “Wavelet-based neural network for power disturbance recognition and classification”, *IEEE Transactions on Power Delivery*, Vol. 19, pp. 1560–1568, 2004.
- [11] M. Uyar, S. Yildirim, M.T. Gencoglu, “An effective wavelet-based feature extraction method for the classification of power quality disturbance signals”, *Electric Power Systems Research*, Vol. 78, pp. 1747–1755, 2008.
- [12] A.M. Gaouda, S.H. Kanoun, M.M.A. Salama, A.Y. Chikhani, “Pattern recognition applications for power system disturbance classification”, *IEEE Transactions on Power Delivery*, Vol. 17, pp. 677–683, 2002.
- [13] H. Adeli, S. Ghosh-Dastidar, N. Dadmehr, “A wavelet-chaos methodology for analysis of EEGs and EEG subbands to detect seizure and epilepsy”, *IEEE Transactions on Biomedical Engineering*, Vol. 54, pp. 205–211, 2007.
- [14] S. Ghosh-Dastidar, H. Adeli, N. Dadmehr, “Mixed-band wavelet-chaos neural network methodology for epilepsy and epileptic seizure detection”, *IEEE Transactions on Biomedical Engineering*, Vol. 54, pp. 1545–1551, 2007.
- [15] I. Omerhodzic, S. Avdakovic, A. Nuhanovic, K. Dizdarevic, “Energy distribution of EEG signals: EEG signal wavelet-neural network classifier”, *Journal of Biological and Life Science*, Vol. 6, pp. 210–215, 2010.
- [16] S. Avdakovic, A. Nuhanovic, M. Kusljagic, M. Music, “Wavelet transform applications in power system dynamics”, *Electric Power Systems Research*, Vol. 83, pp. 237–245, 2012.
- [17] S. Bruno, M. De Benedictis, M. La Scala, “Taking the pulse of power systems: monitoring oscillations by wavelet analysis and wide area measurement system”, *Proceedings of the IEEE-PES Power Systems Conference and Exposition*, pp. 436–443, 2006.
- [18] M. Bronzini, S. Bruno, M. De Benedictis, M. La Scala, “Power system modal identification via wavelet analysis”, *Proceedings of the IEEE Lausanne Power Tech*, pp. 2041–2046, 2007.
- [19] S. Avdakovic, M. Music, A. Nuhanovic, M. Kusljagic, “An identification of active power imbalance using wavelet transform”, *Proceedings of the 9th IASTED European Conference on Power and Energy Systems*, Paper ID 681–019, 2009.
- [20] T. Hashiguchi, H. Ukai, Y. Mitani, M. Watanabe, O. Saeki, M. Hojo, “Power system dynamic performance measured by phasor measurement unit”, *Proceedings of the IEEE Lausanne Power Tech*, pp. 1694–1699, 2007.
- [21] T. Hashiguchi, Y. Mitani, O. Saeki, K. Tsuji, M. Hojo, H. Ukai, “Monitoring power system dynamics based on phasor measurements from demand side outlets developed in the Japan Western 60 Hz system”, *Proceedings of the IEEE/PES Power Systems Conference and Exposition*, Vol. 2, pp. 1183–1189, 2004.
- [22] K. Mei, S.M. Rovnyak, C.M. Ong, “Dynamic event detection using wavelet analysis”, *Proceedings of the IEEE/PES General Meeting*, pp. 1–7, 2006.
- [23] J. Turunen, J. Thambirajah, M. Larsson, B.C. Pal, N.F. Thornhill, L.C. Haarla, W.W. Hung, A.M. Carter, T. Rauhala, “Comparison of three electromechanical oscillation damping estimation methods”, *IEEE Transactions on Power Systems*, Vol. 26, pp. 2398–2407, 2011.
- [24] J.L. Rueda, C.A. Juarez, I. Erlich, “Wavelet-based analysis of power system low-frequency electromechanical oscillations”, *IEEE Transactions on Power Systems*, Vol. 26, pp. 1733–1743, 2011.
- [25] S. Avdakovic, A. Nuhanovic, “Identifications and monitoring of power system dynamics based on the PMUs and wavelet technique”, *International Journal of Electrical and Electronics Engineering*, Vol. 4, pp. 512–519, 2010.

- [26] S. Avdakovic, A. Nuhanovic, M. Kusljugic, E. Becirovic, M. Music, "Identification of low frequency oscillations in power systems", Proceedings of the 6th International Conference on Electrical and Electronics Engineering, pp. 103–107, 2009.
- [27] S. Avdakovic, A. Nuhanovic, M. Kusljugic, "An estimation rate of change of frequency using wavelet transform", International Review of Automatic Control, Vol. 4, pp. 267–272, 2011.
- [28] A.R. Messina, V. Vittal, G.T. Heydt, T.J. Browne, "Nonstationary approaches to trend identification and denoising of measured power system oscillations", IEEE Transactions on Power Systems, Vol. 24, pp. 1798–1807, 2009.
- [29] S. Jaffard, Y. Meyer, R.D. Ryan, Wavelets - Tools for Science and Technology, Philadelphia, PA, USA, Society for Industrial and Applied Mathematics, 2001.
- [30] I. Daubechies, Ten Lectures on Wavelets, Philadelphia, PA, USA, Society for Industrial and Applied Mathematics, 1992.
- [31] M. Vetterli, J. Kovacevic, Wavelets and Subband Coding, New York, Prentice-Hall, 1995.
- [32] S. Mallat, A Wavelet Tour of Signal Processing, San Diego, CA, USA, Academic Press, 1998.
- [33] L. Ekonomou, P. Liatsis, I.F. Gonos, I.A. Stathopoulos, "Artificial neural network-based software tool for calculating the lightning performance of high-voltage transmission lines", IEE Proceedings - Science Measurement and Technology, Vol. 153, pp. 188–193, 2006.
- [34] S. Dreiseitl, L. Ohno-Machado, "Logistic regression and artificial neural network classification models: a methodology review", Journal of Biomedical Informatics, Vol. 35, pp. 352–359, 2002.
- [35] I.A. Basheer, M. Hajmeer, "Artificial neural networks: fundamentals, computing, design, and application", Journal of Microbiological Methods, Vol. 43, pp. 3–31, 2000.
- [36] B.B. Chaudhuri, U. Bhattacharya, "Efficient training and improved performance of multilayer perceptron in pattern classification", Neurocomputing, Vol. 34, pp. 11–27, 2000.
- [37] M.A. Pai, Energy Function Analysis for Power System Stability, Norwell, MA, USA, Kluwer Academic Publishers, 1989.
- [38] M. Nizam, A. Mohamed, A. Hussain, "Voltage collapse prediction incorporating both static and dynamics analyses", European Journal of Scientific Research, Vol. 16, pp. 10–25, 2007.
- [39] F. Milano, PSAT-Power System Analysis Toolbox, Documentation for PSAT Version 1.3.4., 2005, available at <http://thunderbox.uwaterloo.ca/~fmilano>.
- [40] M. Misiti, Y. Misiti, G. Oppenheim, J.M. Poggio, Wavelet Toolbox™ 4 User's Guide, Natick, MA, USA, The MathWorks Inc., 2007.